

# The 125 GeV Higgs boson signal within the Complex NMSSM

S. Moretti<sup>a,†</sup>, S. Munir<sup>b,†</sup> and P. Poullose<sup>c,†</sup>

<sup>a</sup> *School of Physics & Astronomy,  
University of Southampton, Southampton SO17 1BJ, UK.*

<sup>b</sup> *National Centre for Nuclear Research, Hoza 69, 00-681 Warsaw, Poland.*

<sup>c</sup> *Department of Physics,  
IIT Guwahati, Assam 781039, India.*

## Abstract

While the properties of the 125 GeV Higgs boson-like particle observed by the ATLAS and CMS collaborations are largely compatible with those predicted for the Standard Model state, significant deviations are present in some cases. We, therefore, test the viability of a Beyond the Standard Model scenario based on Supersymmetry, the CP-Violating Next-to-Minimal Supersymmetric Standard Model, against the corresponding experimental observations. Namely, we identify possible model configurations in which one of its Higgs bosons is consistent with the LHC observation and evaluate the role of the explicit complex phases on both the mass and di-photon decay of such a Higgs boson. Through a detailed analysis of some benchmark points corresponding to each of these configurations, we highlight the impact of the CP-violating phases on the model predictions compared to the CP-conserving case.

<sup>†</sup>E-mails:

S.Moretti@soton.ac.uk,

SMunir@fuw.edu.pl,

Poullose@iitg.ernet.in.

# 1 Introduction

In July 2012, the CMS and ATLAS experimental collaborations at the Large Hadron Collider (LHC) announced the observation of a new boson [1, 2], consistent with a Higgs particle, the last undiscovered object in the Standard Model (SM). The initial results were based on data corresponding to integrated luminosities of  $5.1 \text{ fb}^{-1}$  taken at  $\sqrt{s} = 7 \text{ TeV}$  and  $5.3 \text{ fb}^{-1}$  at  $8 \text{ TeV}$  and the search was performed in six decay modes:  $H \rightarrow \gamma\gamma, ZZ, Z\gamma, WW, \tau^+\tau^-$  and  $b\bar{b}$ . A  $\sim 5\sigma$  excess of events with respect to the background was clearly observed in the first and second of these decay modes, while the remaining ones yielded exclusion limits well above the SM expectation. Both collaborations have since been regularly updating their findings [3, 4, 5, 6, 7], improving the mass and (so-called) ‘signal strength’ measurements.

In these searches, the magnitude of a possible signal is characterized by the production cross section times the relevant Branching Ratios (BRs) relative to the SM expectations in a given Higgs boson decay channel  $X$ , denoted by  $R(X) = \sigma/\sigma_{\text{SM}} \times \text{BR}(X)/\text{BR}_{\text{SM}}(X)$  (i.e., the signal strength). According to the latest results released by the two collaborations after the collection of  $\sim 20 \text{ fb}^{-1}$  of data [5, 6, 7], a broad resonance compatible with a  $125 \text{ GeV}$  signal is now also visible in the  $WW \rightarrow 2l2\nu$  decay channel. The mass of the observed particle is still centered around  $125 \text{ GeV}$  but the measured values of its signal strength in different channels have changed considerably compared to the earlier results. These values now read

$$R(\gamma\gamma) = 0.78 \pm 0.28, \quad R(ZZ) = 0.91^{+0.3}_{-0.24}, \quad R(WW) = 0.76 \pm 0.21$$

at CMS, and

$$R(\gamma\gamma) = 1.65 \pm 0.35, \quad R(ZZ) = 1.7 \pm 0.5, \quad R(WW) = 1.01 \pm 0.31$$

at ATLAS. The bulk of the event rates comes from the gluon-gluon fusion channel [8]. Furthermore, the signal has also been corroborated by Tevatron analyses [9], covering the  $b\bar{b}$  decay mode only, with the Higgs boson stemming from associated production with a  $W$  boson [8]. However, there the comparisons against the SM Higgs boson rates are biased by much larger experimental errors.

If the current properties of the observed particle are confirmed after an analysis of the full 7 and  $8 \text{ TeV}$  data samples from the LHC, they will not only be a clear signature of a Higgs boson, but also a significant hint for possible physics beyond the SM. In fact, quite apart from noting that the current data are not entirely compatible with SM Higgs boson production rates, while the most significant LHC measurements point to a mass for the new resonance around  $125 \text{ GeV}$  the Tevatron excess in the  $b\bar{b}$  channel points to a range between  $115 \text{ GeV}$  and  $135 \text{ GeV}$ . While the possibility that the SM Higgs boson state has any of such masses would be merely a coincidence (as its mass is a free parameter), in generic Supersymmetry (SUSY) models the mass of the lightest Higgs boson with SM-like behavior is naturally confined to be less than  $180 \text{ GeV}$  or so [10]. The reason is that SUSY, in essence, relates trilinear Higgs boson and gauge couplings, so that the former are of the same size as the latter, in turn implying such a small Higgs boson mass value. Therefore, the new LHC results could well be perceived as being in favor of some low energy SUSY realisation.

Several representations of the latter have recently been studied in connection with the aforementioned LHC and Tevatron data, including the Minimal Supersymmetric Standard Model (MSSM) [11] (also the constrained version [12] of it, in fact), the Next-to-Minimal Supersymmetric Standard Model (NMSSM) [13, 14, 15], the  $E_6$ -inspired Supersymmetric Standard Model ( $E_6\text{SSM}$ ) [16] and the (B-L) Supersymmetric Standard Model ((B-L)SSM) [17]. All of these scenarios can yield a SM-like Higgs boson with mass around  $125 \text{ GeV}$  and most of them can additionally explain the excesses in the signal strength measurements in the di-photon channel.

Another approach to adopt in order to test the viability of SUSY solutions to the LHC Higgs boson data is to consider the possibility of having CP-violating (CPV) phases (for a general review of CP Violation, see [18]) in (some of) the SUSY parameters. These phases can substantially modify

Higgs boson phenomenology in both the mass spectrum and production/decay rates at the LHC [19, 20, 21, 22], while at the same time providing a solution to electroweak baryogenesis [23]. In the context of the LHC, the impact of CPV phases was emphasized long ago in [24, 25] and revisited recently in [26] following the Higgs boson discovery. In all such papers though, CPV effects were studied in the case of the MSSM.

In this paper, we consider the case of similar CPV effects in the NMSSM. In particular, we study the possibility to have Higgs boson signals with mass around 125 GeV in the CPV NMSSM which are in agreement with the aforementioned LHC data as well as the direct search constraints on sparticle masses from LEP and LHC. We also investigate the dependence of the feasible CPV NMSSM signals on the mass of the Higgs boson as well as its couplings to both the relevant particle and sparticle states entering the model spectrum, chiefly, through the decay of the former into a  $\gamma\gamma$  pair. We thus aim at a general understanding of how such observables are affected by the possible complex phases explicitly entering the Higgs sector of the next-to-minimal SUSY Lagrangian.

The paper is organized as follows. In the next section we will briefly review the possible explicit CPV phases in the Higgs sector of the NMSSM. In Sect. 3 we will outline the independent CPV NMSSM parameters and the methodology adopted to confine our attention to the subset of them that can impinge on the LHC Higgs boson data. In the same section, we further investigate the possible numerical values of the complex parameters after performing scans of the low energy CPV NMSSM observables compatible with the LEP and LHC constraints on Higgs boson and SUSY masses. In Sect. 4 we present our results on the Higgs boson mass spectrum as well as signal rates in connection with the LHC. Finally, we conclude in Sect. 5.

## 2 CPV phases in the Higgs sector of the NMSSM

The CPV phases appearing in the Higgs potential of the NMSSM at tree-level [27] can be divided into three categories:

1.  $\theta$  and  $\varphi$ : the spontaneous CPV phases of the vacuum expectation values (vevs) of the up-type Higgs doublet  $H_u$  and the Higgs singlet  $S$ , respectively, with respect to the down-type Higgs doublet  $H_d$ ;
2.  $\phi_\lambda$  and  $\phi_\kappa$ : the phases of the Higgs boson trilinear couplings  $\lambda$  and  $\kappa$ ;
3.  $\phi_{A_\lambda}$  and  $\phi_{A_\kappa}$ : the phases of the trilinear soft terms  $A_\lambda$  and  $A_\kappa$ .

As explained in [28, 29] the phases in 3. above are determined by the minimisation conditions of the Higgs potential with respect to the three Higgs fields. Furthermore, assuming vanishing spontaneous CPV phases in 1. (and real SM Yukawa couplings), the only actual physical phases appearing in the tree-level Higgs potential are those in 2. as the difference  $\phi_\lambda - \phi_\kappa$ . Beyond the Born approximation, the phases of the trilinear couplings  $A_t$ ,  $A_b$  and  $A_\tau$  also enter the Higgs sector through radiative corrections from the third generation squarks and stau (assuming negligible corrections from the first two generations). Also, in the one-loop effective potential,  $\phi_\lambda$  can contribute independently from  $\phi_\kappa$ . The complete one-loop Higgs mass matrix can be found in [28, 29, 30]. Here we only reproduce the tree-level Higgs as well as sfermion mass matrices in Appendix A.

The  $5 \times 5$  Higgs mass matrix  $\mathcal{M}_H^2$  (after rotating out the Goldstone modes) is diagonalized with a unitary matrix  $O$  to yield five mass eigenstates as

$$(H_{dR}, H_{uR}, S_R, H_I, S_I)^T = O (H_1, H_2, H_3, H_4, H_5)^T, \quad (1)$$

where  $O^T \mathcal{M}_H^2 O = \text{diag}(m_{H_1}^2, m_{H_2}^2, m_{H_3}^2, m_{H_4}^2, m_{H_5}^2)$  in order of increasing mass. For a non-zero value of any of the phases listed above, these mass eigenstates become CP-indefinite due to scalar-pseudoscalar mixing. Moreover, these CPV phases not only affect the masses of the Higgs states but also their decay widths, since the Higgs boson couplings to various particles are proportional to the elements of the unitary matrix  $O$  (see, e.g., [31, 32]). Additionally, alterations in the masses of light neutralinos and charginos, in particular, due to the phases in 1. above can also have an indirect impact on the BRs of the Higgs bosons into SM particles.

The decay widths and BRs of the Higgs boson in the NMSSM with CPV phases can be calculated using the methodology implemented in [31]. Explicit expressions for Higgs boson couplings and widths in the CPV NMSSM can be found in [33], which follows the notation of [34]. These widths and BRs can then be used to obtain the signal strength of the  $\gamma\gamma$  channel (also called *reduced* di-photon cross section),  $R_{H_i}^{\gamma\gamma}$ , defined, for a given Higgs boson,  $H_i$ , as

$$R_{H_i}^{\gamma\gamma} = \frac{\sigma(gg \rightarrow H_i)}{\sigma(gg \rightarrow H_{\text{SM}})} \times \frac{\text{BR}(H_i \rightarrow \gamma\gamma)}{\text{BR}(H_{\text{SM}} \rightarrow \gamma\gamma)}, \quad (2)$$

where  $H_{\text{SM}}$  implies a SM Higgs boson with the same mass as  $H_i$ . In terms of the *reduced* couplings,  $C_i(X)$  (couplings of  $H_i$  with respect to those of  $H_{\text{SM}}$ ), eq. (2) can be approximated by

$$R_{H_i}^{\gamma\gamma} = [C_i(gg)]^2 [C_i(\gamma\gamma)]^2 \sum_X \frac{\Gamma_{h_{\text{SM}}}^{\text{total}}}{\Gamma_{H_i}^{\text{total}}} \quad (3)$$

where  $\Gamma_{h_{\text{SM}}}^{\text{total}}$  denotes the total width of  $H_{\text{SM}}$ .

### 3 Model parameters and methodology

In light of the recent LHC discovery of a SM Higgs boson-like particle we scan the parameter space of the CPV Higgs sector of the NMSSM using a newly developed FORTRAN code. In our scans the LEP constraints on the model Higgs bosons are imposed in a modified fashion, i.e., they have to be satisfied by the scalar and pseudoscalar components of all the CP-mixed Higgs bosons. Also imposed are the constraints from the direct searches of the third generation squarks, stau and the light chargino at LEP. We point out here that, in the CP-conserving (CPC) limit, the Higgs boson mass and BRs have been compared with those given by NMSSMTools [35] and have been found to differ from the latter by  $\sim 1\%$  and  $\sim 5\%$  at the most, respectively. Although no limits from  $b$ -physics or from relic density measurements have been imposed we confine ourselves to the regions the parameter space regions which have been found to comply with such constraints (see, e.g., [15]).

We study the effects of the CPV phases described in the previous section on the mass and di-photon signal rate of a Higgs boson predicted by the model that is compatible with the Higgs boson discovery data from the LHC. In particular, we consider three most likely scenarios specific to the CPV NMSSM that comply with the latter. In our analysis, we assume minimal Supergravity (mSUGRA)-like unification of the soft parameters at the SUSY-breaking energy scale, such that

$$\begin{aligned} M_0 &\equiv M_{Q_3} = M_{U_3} = M_{D_3} = M_{L_3} = M_{E_3} = M_{\text{SUSY}}, \\ M_{1/2} &\equiv 2M_1 = M_2 = \frac{1}{3}M_3, \\ A_0 &\equiv A_t = A_b = A_\tau, \end{aligned}$$

where  $M_{Q_3}^2$ ,  $M_{U_3}^2$ ,  $M_{D_3}^2$  and  $M_{L_3}^2$ ,  $M_{E_3}^2$  are the soft SUSY-breaking squared masses of the third generation squarks and sleptons, respectively. These parameters are then fixed to their optimal values based on earlier studies [13, 15] in order to minimise the set of scanned parameters. We then

focus only on the effects of the Higgs sector parameters, which include the dimensionless Higgs boson couplings  $\lambda$  and  $\kappa$  along with their phases  $\phi_\lambda$  and  $\phi_\kappa$ , as well as the soft SUSY-breaking parameters  $A_\lambda$  and  $A_\kappa$ . From outside the Higgs sector, we only analyse the effect of the variation of the unified CPV phase of the third generation trilinear couplings,  $\phi_{A_0}$  ( $\equiv \phi_{A_t} = \phi_{A_b} = \phi_{A_\tau}$ ).

Before we discuss the three scenarios mentioned above, we note that the two heaviest Higgs boson mass eigenstates  $H_4$  and  $H_5$  always correspond to the interaction eigenstates  $H_{uR}$  and  $H_I$  in eq. (1).<sup>1</sup> Hence, a Scenario is defined by the Higgs state that conforms to the LHC observations, out of the three light mass eigenstates,  $H_1$ ,  $H_2$  and  $H_3$ , and by the correspondence between the latter and the interaction eigenstates  $H_{dR}$ ,  $S_R$  and  $S_I$ . However, note that such a definition is adopted only so that a distinction between different Scenarios can be made conveniently. Evidently, the behavior of the ‘observed’ Higgs boson,  $H_{\text{sig}}$ , with the CPV phases in a given Scenario is a combined result of the set of parameters yielding that Scenario rather than of its position among the mass-ordered Higgs states. The criteria for choosing the ranges of the scanned model parameters as well as the values of the non-Higgs-sector SUSY parameters thus depend on the Scenario under consideration and are explained in the following.

Scenario 1: In this Scenario the lightest Higgs state,  $H_1$ , is the SM-like one and corresponds to  $H_{dR}$ , while  $H_2$  and  $H_3$  correspond to  $S_R$  and  $S_I$ , respectively. The requirement of obtaining a down-type Higgs state with mass close to 125 GeV and with SM-like couplings necessitates large soft SUSY masses and  $A_0$ . The values of  $\mu_{\text{eff}}$  ( $\equiv \lambda s$ , where  $s$  is the vev of  $S$ ) and the gaugino masses are found to be in best agreement with the relic density constraints [15], giving a neutralino with a large higgsino component as the lightest SUSY particle. Further,  $\lambda$  and  $\kappa$  are chosen such that there is enough mixing of the doublet with the singlet Higgs boson so as to allow an  $H_1$  with the correct mass while keeping its couplings close to their SM values. We test two Cases for this Scenario, corresponding to two representative values of the parameter  $\tan\beta$  ( $\equiv v_u/v_d$ , where  $v_u$  and  $v_d$  are the vevs of  $H_u$  and  $H_d$ , respectively), which is fixed to 8 in Case 1 and to 15 in Case 2.

Scenario 2: This Scenario is defined by the SM-like  $\sim 125$  GeV Higgs boson being the second lightest Higgs boson,  $H_2$ , of the model. There are two possibilities entailing such a Scenario. It can correspond to  $S_R$  in which case it has  $R_{H_i}^{\gamma\gamma}$  SM-like or bigger, as shown in [13]. We refer to this possibility as Case 1 of this Scenario. It requires relatively large values of  $\lambda$  and  $\kappa$ , small values of the parameters  $A_\lambda$  and  $A_\kappa$  and moderate values of soft SUSY-breaking parameters.  $H_1$  and  $H_3$  in this Case are  $H_{dR}$ - and  $S_I$ -like, respectively. For Case 2 of this Scenario, we take a slightly different region of the parameter space which yields a  $H_2$  that is  $H_{dR}$ -like and hence has  $R_{H_2}^{\gamma\gamma}$  around the SM expectation. Therefore, heavy unified soft squark mass and/or trilinear coupling are required in this Case, but a light soft gaugino mass is preferred.  $\lambda$  can be small to intermediate while  $\kappa$  is always small. Finally,  $H_1$  and  $H_3$  are  $S_R$ - and  $S_I$ -like, respectively.

Scenario 3: There also exists the possibility that the observed  $\sim 125$  GeV Higgs boson is the  $H_3$  of the model which corresponds to  $H_{dR}$ , while both  $S_R$ - and  $S_I$ -like Higgs bosons are lighter. Such a Scenario can be realized for very fine-tuned ranges of the parameters  $A_\lambda$  and  $A_\kappa$  for a given  $\tan\beta$  value, with large soft squark and gaugino mass parameters preferred. Note that in this Case the  $S_I$ -like  $H_3$  of Case 2 of Scenario 2 turns into  $H_2$  by becoming lighter than the  $H_{dR}$ -like state which, consequently, turns into  $H_3$ . These two Cases thus overlap slightly in terms of the relevant

---

<sup>1</sup>Implying that after diagonalization of the Higgs mass matrix, e.g.,  $H_4$  sits in the position corresponding to  $H_{uR}$  in eq. (1) before ordering by mass, even though evidently it contains components of the other Higgs fields also. In particular, a SM-like  $H_i$  contains adequate components of both  $H_{uR}$  and  $H_{dR}$  to have SM-like couplings to fermions and gauge bosons.

Scenario	1, Case 1	1, Case 2	2, Case 1	2, Case 2	3
Fixed parameters					
$M_0$ (TeV)	5		0.8	3	3
$M_{1/2}$ (TeV)	3		0.35	0.35	1.5
$-A_0$ (TeV)	10		1	4	4
$\mu_{\text{eff}}$ (TeV)	1		0.14	0.14	0.14
$\tan \beta$	6	15	1.9	20	10
Scanned parameters					
$\lambda$	0.01 – 0.1		0.5 – 0.6	0.01 – 0.3	0.1 – 0.3
$\kappa$	0.1 – 0.3		0.3 – 0.4	0.01 – 0.1	0.05 – 0.1
$A_\lambda$ (TeV)	1.5 – 3		0.14 – 0.2	0.2 – 0.6	0.95 – 1.05
$-A_\kappa$ (TeV)	1 – 4		0.2 – 0.25	0.1 – 0.3	0.07 – 0.09

Table 1: Input parameters of the CPV NMSSM and their numerical values adopted in our analysis.

parameter space of the model.

Note here that we do not consider a scenario with the  $\sim 125$  GeV Higgs boson corresponding to the  $S_I$  interaction eigenstate, since the pure (or nearly pure) pseudoscalar hypothesis is disfavored by the CMS Higgs boson analyses [36, 37]. Values of the fixed parameters as well as ranges of the variable parameters for all the above Scenarios are given in Tab. 1.

## 4 Scans and results

We perform scans for each of the scenarios described earlier requiring the mass of  $H_{\text{sig}}$  (i.e., of  $H_1$  in Scenario 1,  $H_2$  in Scenario 2 and  $H_3$  in Scenario 3) to lie in the range  $124 \text{ GeV} < m_{H_{\text{sig}}} < 127 \text{ GeV}$ .<sup>2</sup> We additionally impose the condition  $R_{H_{\text{sig}}}^{\gamma\gamma} > 0.5$  on the signal Higgs boson. Furthermore, to each Case in a given Scenario corresponds a set of three scans, such that in each of the scans only one of the following CPV phases is varied:

- (i)  $\phi_\kappa$ , (ii)  $\phi_\lambda$ , (iii)  $\phi_{A_0}$ ,

while fixing the others to  $0^\circ$ . Each scan thus checks the effect of a different CPV source at the tree-level and/or beyond. In each scan we vary the relevant phase in steps of  $1^\circ$  between  $0^\circ - 180^\circ$ .

The measurements of the Electric Dipole Moment (EDM) of the electron, neutron and various atoms [38, 39, 40] put constraints on the allowed values of  $\phi_\lambda$  and  $\phi_{A_0}$ . However, the trilinear couplings of squarks and sleptons contribute to the EDMs only at the two-loop level and their phases are thus rather weakly constrained. One can, furthermore, assign very heavy soft masses to the sfermions of first two generations in order to minimize the effect of  $\phi_{A_0}$  on the EDMs, as pointed out in earlier studies for the MSSM [41]. In fact, such constraints can be neglected altogether by arguing that the phase combinations occurring in the EDMs can be different from the ones inducing Higgs boson mixing [42]. The phase of  $\kappa$ , in contrast, has been found to be virtually unconstrained by the EDM measurements [32, 29].

Below we present our results separately for each of the five Cases investigated. For evaluating the effect of the phases on  $m_{H_{\text{sig}}}$  and  $R_{H_{\text{sig}}}^{\gamma\gamma}$  qualitatively, we choose a set of four Representative

<sup>2</sup>We thus use the central mass measurement of 125.5 GeV in accordance with the CMS results.

Points (RPs), referred to as RP1, RP2, RP3 and RP4 in the following, for every Case. As explained in Sect. 2, at the tree-level the only independent CPV phase entering the Higgs mass matrix is the difference  $\phi_\lambda - \phi_\kappa$ . At one-loop level, although  $\phi_\lambda$  can appear separately from  $\phi_\kappa$ , the contribution from the corresponding terms is much smaller than the tree-level dependence on  $\phi_\lambda - \phi_\kappa$ . Furthermore, since only  $\cos(\phi_\lambda - \phi_\kappa)$  appears in the diagonal CP-even and CP-odd blocks and only  $\sin(\phi_\lambda - \phi_\kappa)$  in the CP-mixing block (see Appendix A) of the Higgs mass matrix, the mass eigenstates show a very identical behavior when either of these two phases is varied while fixing the other to  $0^\circ$ . Only small differences arise for very large values of  $\phi_\lambda$  and  $\phi_\kappa$  due to the higher order corrections. Therefore, our RP1 for a given Case corresponds to a point for which the effect of  $\phi_\lambda$  (and equivalently  $\phi_\kappa$ ) on  $m_{H_{\text{sig}}}$  is maximised for that Case. Similarly, RP3 is chosen such that the variation in  $m_{H_{\text{sig}}}$  is maximal with  $\phi_{A_0}$ , since this phase only appears at the one-loop level and can potentially cause a behavior different from that due to the tree-level CPV phase. The dependence on  $\phi_{A_0}$  can, however, be expected to show an identical behavior across all Cases, as it is largely independent of other Higgs sector parameters (except  $\tan\beta$ ), which is indeed what we will observe in our results below.

As already noted, the CPV phases also affect the Higgs boson decay widths into fermions and gauge bosons, through the elements of the Higgs mixing matrix  $O$ . On the other hand, in the decays of a Higgs boson into two lighter Higgs bosons the tree-level phase,  $\phi_\lambda - \phi_\kappa$ , enters directly while the phase  $\phi_{A_0}$  also enters through the one-loop CP-odd tadpole conditions at one-loop [28, 33]. RP2 and RP4 are, therefore, points with the largest effect on  $R_{H_{\text{sig}}}^{\gamma\gamma}$  due to the variation in  $\phi_\lambda/\phi_\kappa$  and  $\phi_{A_0}$ , respectively, observed in our scans. Note that in the discussion below the description of the behavior of a given RP may not be equally applicable to all other good points, since it is chosen only so as to understand the maximum possible impact of a given phase and to highlight some potentially distinguishing features of different Cases and Scenarios.

#### 4.1 Scenario 1:

Case 1: In Fig. 1a we show, for the small  $\tan\beta$  case of this Scenario, the variation in the number of good points, i.e., points surviving the conditions imposed on  $m_{H_{\text{sig}}}$  and  $R_{H_{\text{sig}}}^{\gamma\gamma}$ , with varying  $\phi_\lambda$  and  $\phi_\kappa$ . The number of surviving points first falls slowly with increasing  $\phi_\lambda/\phi_\kappa$  and then abruptly for  $\phi_\lambda/\phi_\kappa = 5^\circ$  after which it remains almost constant for a while before falling further. The number of surviving points reduces to 0 for  $\phi_\lambda$  and  $\phi_\kappa$  larger than  $75^\circ$  and  $77^\circ$ , respectively. However, very few,  $\sim 10$ , surviving points reemerge for  $\phi_\lambda$  and  $\phi_\kappa$  larger than  $155^\circ$  and  $150^\circ$ , respectively, although it is not apparent from the Figure. The drop in the number of points is not continuous since there are other parameters,  $\lambda$ ,  $\kappa$ ,  $A_\lambda$  and  $A_\kappa$ , which are also scanned over for every value of a given phase. Moreover, the number of good points evidently depends on the conditions on  $m_{H_{\text{sig}}}$  and  $R_{H_{\text{sig}}}^{\gamma\gamma}$  so that while both of these may be satisfied for one value of a phase one of these may be violated for the next. Although, as we shall see below,  $m_{H_{\text{sig}}}$  is almost always mainly responsible for the drop in the number of good points.

Note that the CPC case is also subject to the conditions on  $m_{H_{\text{sig}}}$  and  $R_{H_{\text{sig}}}^{\gamma\gamma}$  and, on account of being defined relative to this Case, the number of good points does not represent all possible solutions for all values of the phases. Thus, it is likely that the CPC case for a given parameter set falls outside the defined ranges of  $m_{H_{\text{sig}}}$  and/or  $R_{H_{\text{sig}}}^{\gamma\gamma}$ , but the conditions on these are satisfied for a different value of a particular phase. Such a value of the phase can thus result in a considerable number of good points which would be absent in the CPC case. Nevertheless, the aim here is to give an estimate of the effect of the CPV phases on the number of good points relative to the CPC case, rather than to present a truly holistic picture. Fig. 1b shows the variation in the number of surviving points with that in  $\phi_{A_0}$ . Contrary to the case of  $\phi_\lambda/\phi_\kappa$ , for this phase the number of

surviving points falls abruptly to 0 when  $\phi_{A_0}$  crosses  $25^\circ$  and then rises again when  $\phi_{A_0}$  reaches  $142^\circ$ . The values of other parameters corresponding to each RP for this Case are given below.

Point	$\lambda$	$\kappa$	$A_\lambda$ (GeV)	$A_\kappa$ (GeV)
RP1	0.091	0.13	1833	-1000
RP1	0.091	0.13	1667	-1000
RP3	0.1	0.26	3000	-4000
RP4	0.01	0.23	2667	-1000

Fig. 1c for RP1 verifies our statement above that the condition on  $m_{H_{\text{sig}}}$  is the one mainly responsible for the drop in the number of good points. This is particularly true for this Case due to the fact that maximum  $m_{H_1}$  obtainable for  $\phi_\kappa/\phi_\lambda = 0^\circ$  already lies not far above the allowed lower limit and the former falls further with increasing values of these phases. Note in the Figure that for very large values of  $\phi_\lambda$  and  $\phi_\kappa$   $m_{H_1}$  rises above the lower limit again, more so for the latter than the former. The variation in  $m_{H_1}$  with increasing  $\phi_{A_0}$  is relatively sharp, as seen in Fig. 1d for RP3. This is due to the fact that in order to reach values up to 125 GeV, the mass of  $H_1$  strongly relies on the trilinear coupling  $A_0$  and is consequently also more sensitive to its phase. Also, while  $m_{H_{\text{sig}}}$  falls initially with increasing  $\phi_{A_0}$ , it appears to reach a minimum for a certain (intermediate) value of  $\phi_{A_0}$  after which it starts rising again. This rise is in fact faster than the earlier drop and as a result  $m_{H_1}$  for RP2 is larger for  $\phi_{A_0} = 180^\circ$  than for  $\phi_{A_0} = 0^\circ$ .

Fig. 1e corresponds to RP2 and shows the dependence of  $R_{H_{\text{sig}}}^{\gamma\gamma}$  on  $\phi_\lambda$  and  $\phi_\kappa$  for this Case. We note that  $R_{H_{\text{sig}}}^{\gamma\gamma}$  falls very slowly with an increase in the value of either of these phases, deviating from the CPC case only at a percent level for  $\phi_\lambda/\phi_\kappa \sim 180^\circ$  but still staying very SM-like. The large break in the line corresponds to those values of the phases for which  $m_{H_1}$  for this RP falls below the allowed range in analogy with RP1 in Fig. 1c above. The observed behavior of  $R_{H_{\text{sig}}}^{\gamma\gamma}$  is due to the fact that with increasing values of  $\phi_\lambda/\phi_\kappa$  while  $\text{BR}(H_1 \rightarrow b\bar{b})$  drops and  $\text{BR}(H_1 \rightarrow \gamma\gamma)$  rises, there is a drop in  $\Gamma(H_1 \rightarrow gg)$  also (see Eq. (2)), resulting in an overall (slight) reduction in  $R_{H_{\text{sig}}}^{\gamma\gamma}$ . Conversely, for very large values of  $\phi_\lambda$  and  $\phi_\kappa$  the drop in  $R_{H_{\text{sig}}}^{\gamma\gamma}$  is even more significant because  $\text{BR}(H_1 \rightarrow b\bar{b})$  ( $\text{BR}(H_1 \rightarrow \gamma\gamma)$ ) is slightly larger (smaller) than its value in the CPC case. Finally, Fig. 1f for RP4 shows that  $R_{H_{\text{sig}}}^{\gamma\gamma}$  has negligible dependence on  $\phi_{A_0}$ , since for the range of the latter allowed by the condition on  $m_{H_{\text{sig}}}$  the total decay width of  $H_1$  as well as  $\text{BR}(H_1 \rightarrow b\bar{b})$  fall negligibly.

Case 2: For large  $\tan \beta$  in Scenario 1 the drop in the number of good points is slightly slower than in Case 1 with increasing  $\phi_\lambda/\phi_\kappa$  although it follows a similar trend overall, as seen in Fig. 2a. However, there is one notable distinction: the number of surviving points in fact never falls to 0 for the entire range of  $\phi_\kappa$  (although only about 100 points survive for  $\phi_\kappa > 81^\circ$ ) while for a narrow range of  $\phi_\lambda$  not a single point survives the imposed conditions. The reason for this will be explained below. A behavior similar to the Case 1 is also observed in Fig. 2b where the number of good points falls to 0 for a relatively narrower range of  $\phi_{A_0}$ . The RPs for this Case are as follows.

Point	$\lambda$	$\kappa$	$A_\lambda$ (GeV)	$A_\kappa$ (GeV)
RP1	0.086	0.12	1500	-4000
RP2	0.086	0.12	1500	-3000
RP3	0.01	0.3	3000	-4000
RP4	0.095	0.12	1500	-1000



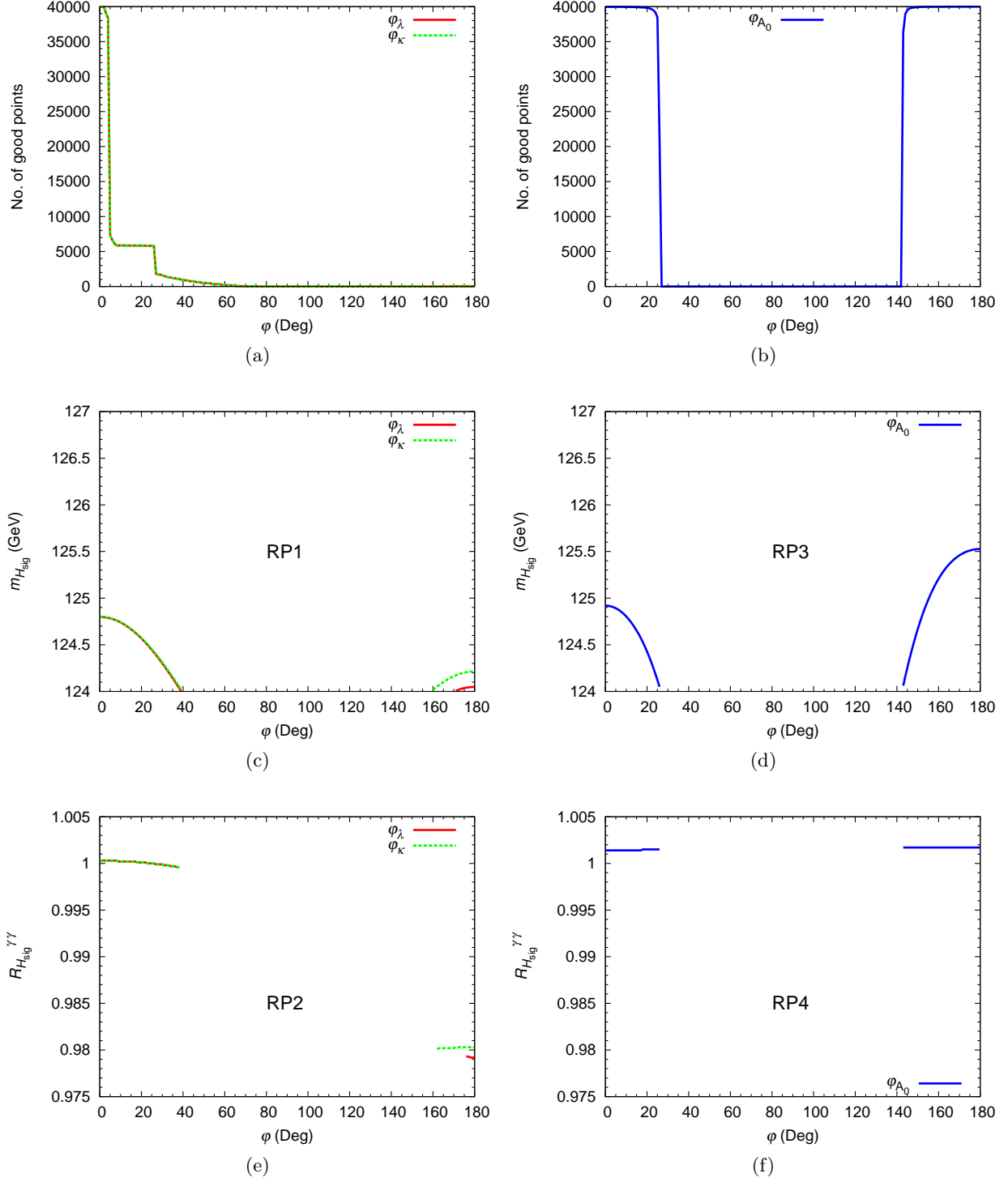


Figure 1: Distributions of good points,  $m_{H_{\text{sig}}}$  and  $R_{H_{\text{sig}}}^{\gamma\gamma}$  for Scenario 1, Case 1.

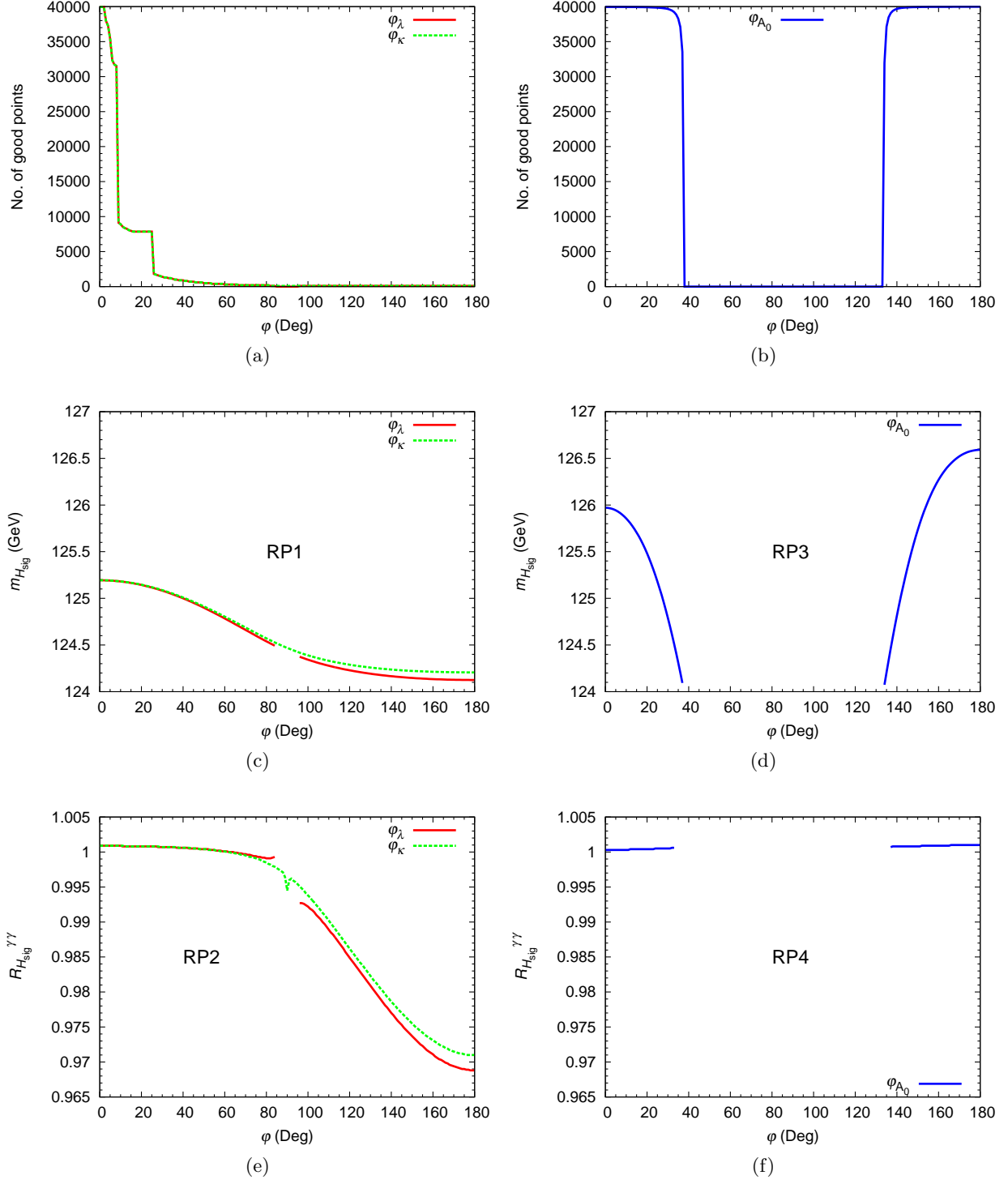


Figure 2: Distributions of good points,  $m_{H_{\text{sig}}}$  and  $R_{H_{\text{sig}}}^{\gamma\gamma}$  for Scenario 1, Case 2.

The sudden drop in the number of good points is, once again, largely driven by  $m_{H_{\text{sig}}}$  which falls gradually with increasing  $\phi_\lambda$  and  $\phi_\kappa$ , as seen in Fig. 2c for RP1. However, this particular RP is one of the few points for which the entire range of  $\phi_\kappa$  is allowed since  $m_{H_1}$  never hits the imposed lower limit. Notice the small break in the line corresponding to  $\phi_\lambda$  despite the lower limit on  $m_{H_1}$  being satisfied, which results from the falling of the mass of the lightest chargino,  $\chi_1^\pm$ , below the LEP limit ( $m_{\chi_1^\pm} > 94 \text{ GeV}$  [43]) for this range of  $\phi_\lambda$ . This in turn causes the number of surviving points to fall to 0 for some intermediate values of  $\phi_\lambda$ , as seen above. Note that this does not happen for  $\phi_\kappa$  as this phase does not enter the chargino mass matrix directly, contrary to  $\phi_\lambda$  (see Appendix A). Fig. 2d for RP3 shows that  $m_{H_1}$  in this Case can reach comparatively higher values than in Case 1, due to larger  $\tan\beta$ , but its variation with increasing  $\phi_{A_0}$  follows the same trend.

$R_{H_{\text{sig}}}^{\gamma\gamma}$  for RP2, shown in Fig. 2e, again follows the same trend with increasing  $\phi_\lambda/\phi_\kappa$  as in Case 1, except that the line corresponding to  $\phi_\lambda$  has a relatively small break (which by contrast is due to the violation of the LEP constraint here). On the other hand, the line corresponding to  $\phi_\kappa$ , while being continuous, has a small kink around  $\phi_\kappa = 90^\circ$ , where the mass of the lightest singlet-like neutralino,  $\chi_1^0$ , becomes small enough to kinematically allow decay of  $H_1$  into its pair. This causes a small drop in the BRs of  $H_1$  into all SM particles. Note that, besides  $\phi_\lambda$ ,  $\phi_\kappa$  also enters the neutralino mass matrix directly, as opposed to the chargino mass matrix. Fig. 2f for RP4 of this Case shows a slightly larger (although still negligible) enhancement in  $R_{H_{\text{sig}}}^{\gamma\gamma}$  with increasing  $\phi_{A_0}$  as compared to that in the Case 1.

We should mention here that  $H_2$  and  $H_3$  are always very heavy,  $\sim 1 \text{ TeV}$  and  $\sim 2 \text{ TeV}$ , respectively, for both the Cases of this Scenario. Moreover,  $R_{H_{\text{sig}}}^{ZZ}$  follows the same trend with the variation in CPV phases as  $R_{H_{\text{sig}}}^{\gamma\gamma}$  and is in fact always almost equal to it. Some important numbers corresponding to these Cases and to the four RPs in each of them are provided in Tab. 2.

## 4.2 Scenario 2:

Case 1: In Fig. 3a we show the number of good points against the phases  $\phi_\lambda$  and  $\phi_\kappa$  for this Case. We see that the number of surviving points for  $\phi_\lambda/\phi_\kappa = 0^\circ$  is much smaller compared to that in the two Cases of Scenario 1. Moreover, there is comparatively an even steeper drop in the number of surviving points with increasing  $\phi_\lambda$  and  $\phi_\kappa$ . In fact, the number of surviving points falls to 0 for  $\phi_\lambda/\phi_\kappa$  as low as  $14^\circ$ , owing again to the sensitivity of  $m_{H_2}$  to these phases, and it stays 0 for their larger values. The number of surviving points, on the other hand, never falls below  $\sim 1250$  for the entire range of  $\phi_{A_0}$ , as seen in Fig. 3b. In fact, the number of good points falls slowly with increasing  $\phi_{A_0}$ , becomes almost constant with the latter between  $\sim 70^\circ$  and  $\sim 110^\circ$ , and then starts rising again so that for  $\phi_{A_0} = 180^\circ$  it is even larger than in the CPC case. The particulars of the RPs for this Case are given below.

Point	$\lambda$	$\kappa$	$A_\lambda (\text{GeV})$	$A_\kappa (\text{GeV})$
RP1	0.558	0.36	187	-228
RP2	0.511	0.34	173	-222
RP3	0.516	0.33	187	-200
RP4	0.553	0.36	173	-217

$m_{H_{\text{sig}}}$  in this Case can easily reach the defined upper limit of  $127 \text{ GeV}$  when CP is conserved but falls very abruptly with increasing  $\phi_\lambda/\phi_\kappa$ , as shown for RP1 in Fig. 3c. The reason is that this Case corresponds to larger values of  $\lambda$  and  $\kappa$  compared to any other Case discussed here

Scenario	1, Case 1	1, Case 2
Points scanned for each $\phi_\kappa$ or $\phi_\lambda$ or $\phi_{A_0}$	40000	
Points surviving for $\phi_\kappa = \phi_\lambda = \phi_{A_0} = 0$	39961	39954
Min. points surviving, with $\phi_\kappa$	0, 78-144	100, 82-180
Max. points surviving, with $\phi_\kappa$	39961, 0-2	39954, 0-2
Min. points surviving, with $\phi_\lambda$	0, 76-155	0, 85-95
Max. points surviving, with $\phi_\lambda$	39961, 0-2	39954, 0-2
$m_{h_{\text{sig}}}$ for RP1 with $\phi_\kappa = \phi_\lambda = 0$	124.7990	125.1936
$R_{H_{\text{sig}}}^{\gamma\gamma}$ for RP2 with $\phi_\kappa = \phi_\lambda = 0$	1.0003	1.0010
Min. $m_{h_{\text{sig}}}$ obtained for RP1, with $\phi_\kappa$	124.0159, 160	124.2068, 180
Min. $R_{H_{\text{sig}}}^{\gamma\gamma}$ obtained for RP2, with $\phi_\kappa$	0.9801, 162	0.9710, 180
Min. $m_{h_{\text{sig}}}$ obtained for RP1, with $\phi_\lambda$	124.0058, 39	124.1254, 180
Min. $R_{H_{\text{sig}}}^{\gamma\gamma}$ obtained for RP2, with $\phi_\lambda$	0.9792, 180	0.9688, 180
Min. points surviving, with $\phi_{A_0}$	0, 27-142	0, 38-133
Max. points surviving, with $\phi_{A_0}$	39987, 171-180	39973, 171-180
$m_{h_{\text{sig}}}$ for RP3 with $\phi_{A_0} = 0$	124.9199	125.9711
$R_{H_{\text{sig}}}^{\gamma\gamma}$ for RP4 with $\phi_{A_0} = 0$	1.0014	1.0003
Min. $m_{h_{\text{sig}}}$ obtained for RP3, with $\phi_{A_0}$	124.0502, 26	124.0737, 134
Max. $m_{h_{\text{sig}}}$ obtained for RP3, with $\phi_{A_0}$	125.5270, 180	126.5914, 180
Max. $R_{H_{\text{sig}}}^{\gamma\gamma}$ obtained for RP4, with $\phi_{A_0}$	1.0017, 180	1.0010, 180

Table 2: Scan results for Scenario 1, Cases 1 and 2. All angles are in degrees.

and, consequently, the dependence on their phases is more pronounced. In Fig. 3d we show the dependence of  $m_{H_2}$  on  $\phi_{A_0}$  for RP3. While  $m_{H_{\text{sig}}}$  here stays above the imposed lower limit for all values of  $\phi_{A_0}$ , in contrast with what was observed for Scenario 1, its overall behavior is quite similar.  $m_{H_{\text{sig}}}$  again falls continuously with increasing  $\phi_{A_0}$  until some intermediate value of the latter and then starts rising, reaching a value for  $\phi_{A_0} = 180^\circ$  that is larger than the value for the CPC case. Note that in this Case also it is also possible to find points with  $m_{H_{\text{sig}}}$  falling as sharply and reaching the imposed lower limit with not too large  $\phi_{A_0}$ , as was seen in Scenario 1. However, our selected RP3 demonstrates well the possibility of the entire range of  $\phi_{A_0}$  being allowed, which is precluded in Scenario 1.

Fig. 3e for RP2 shows that while  $R_{H_{\text{sig}}}^{\gamma\gamma}$  can be much higher than the SM expectation for the CPC case, the drop in it is very steep with increasing  $\phi_\lambda/\phi_\kappa$ . This is because the total width of  $H_2$  falls sharply owing again to the fact that  $\phi_\lambda$  and  $\phi_\kappa$  have fairly large absolute values. This in fact results in an increase in both  $\text{BR}(H_1 \rightarrow gg)$  and  $\text{BR}(H_1 \rightarrow \gamma\gamma)$  compared to the CPC case, but since the former rises faster than the latter it causes an overall drop in  $R_{H_{\text{sig}}}^{\gamma\gamma}$ . Fig. 3f for RP4 shows an initially slow but eventually sharp drop in  $R_{H_{\text{sig}}}^{\gamma\gamma}$  with increasing  $\phi_{A_0}$  until the latter reaches its intermediate values when  $R_{H_{\text{sig}}}^{\gamma\gamma}$  starts rising again. The main reason for the initial slow drop with increasing  $\phi_{A_0}$  is a slight increase in  $\text{BR}(H_1 \rightarrow gg)$  and for the later sharp drop is an increase in the dominant  $\text{BR}(H_1 \rightarrow b\bar{b})$  and a decrease in  $\text{BR}(H_1 \rightarrow \gamma\gamma)$  itself. Evidently, this behavior is reversed after  $\phi_{A_0} = 90^\circ$ , when  $R_{H_{\text{sig}}}^{\gamma\gamma}$  starts rising again. Finally,  $R_{H_{\text{sig}}}^{ZZ}$  in this Case is always considerably lower than  $R_{H_{\text{sig}}}^{\gamma\gamma}$  (e.g., it is  $\sim 0.7$  for the CPC case of RP2) but shows a similar behavior with varying CPV phases.

Case 2: The composition of  $H_2$  in this Case is closer to that of  $H_1$  in Scenario 1 than to  $H_2$  in Case 1 of this Scenario above (due to smaller  $\lambda$  and consequently smaller singlet component) state. However, Fig. 4a shows a somewhat different behavior from Scenario 1, as the number of good points, though comparatively much smaller for the CPC case, falls very slightly over the entire range of  $\phi_\kappa$ . For  $\phi_\lambda$  between  $60^\circ$  and  $120^\circ$ , the number of points is reduced to 0 due again to the violation of the LEP limit on  $m_{\chi_1^\pm}$ . The behavior of the number of good points with increasing  $\phi_{A_0}$ , on the other hand, is very similar to the Case 1 of this Scenario, as seen in Fig. 4b since for a large number of points  $m_{H_{\text{sig}}}$  stays within the imposed limits for the entire range of  $\phi_{A_0}$ . Below we give the values of other Higgs sector parameters for the four RPs of this Case.

Point	$\lambda$	$\kappa$	$A_\lambda$ (GeV)	$A_\kappa$ (GeV)
RP1	0.043	0.015	200	-160
RP2	0.047	0.011	600	-140
RP3	0.044	0.017	289	-180
RP4	0.036	0.014	422	-173

Fig. 4c for RP1 shows that, contrary to all the Cases discussed so far,  $m_{H_{\text{sig}}}$  rises, albeit slowly, with increasing  $\phi_\lambda/\phi_\kappa$ . The reason is the mixing with the  $S_R$ -like  $H_1$ , the mass of which falls with increasing values of these phases. This is in contrast with Scenario 1 but in fact in analogy with the Case 1 of this Scenario in that there also the mass of the  $H_{dR}$ -like  $H_1$  rises while the mass of the  $S_R$ -like  $H_2$  falls with increasing amount of CP-violation. The dependence of  $m_{H_{\text{sig}}}$  on  $\phi_{A_0}$  for RP3, shown in Fig. 4c, is still similar to what has been observed so far. Note again that while for this particular RP  $m_{H_{\text{sig}}}$  touches the allowed upper limit for the CPC case and drops sharply to the lower limit, thus excluding a wide range of  $\phi_{A_0}$ , points similar to RP3 of the Case 1 above (with the entire range of  $\phi_{A_0}$  allowed) are also available.

In Fig. 4e we show the variation in  $R_{H_{\text{sig}}}^{\gamma\gamma}$  with  $\phi_\lambda$  and  $\phi_\kappa$  for RP2 of this Case. When CP is conserved in this Case  $R_{H_{\text{sig}}}^{\gamma\gamma}$  is generally slightly lower than 1 (SM expectation) but still lies well within the observed range taking into account the experimental uncertainties, reported by the CMS collaboration [5]. The behavior of  $R_{H_{\text{sig}}}^{\gamma\gamma}$ , which falls slowly with increasing  $\phi_\lambda/\phi_\kappa$ , is, however, remarkably similar to that observed in Scenario 1 (notice the relatively compressed scale of the y-axis in the Figure). With increasing but small (very large)  $\phi_{A_0}$  on the other hand,  $R_{H_{\text{sig}}}^{\gamma\gamma}$  falls (rises) a little faster than what has been noted for earlier Cases, as seen in Fig. 4f for RP4. This is due to the fact that, conversely to the earlier Cases, with increasing (but small)  $\phi_{A_0}$ , the dominant  $\text{BR}(H_1 \rightarrow b\bar{b})$  increases gradually while  $\text{BR}(H_1 \rightarrow \gamma\gamma)$  itself falls very slowly, and vice versa for very large  $\phi_{A_0}$ . Once again,  $R_{H_{\text{sig}}}^{ZZ}$  is very close to  $R_{H_{\text{sig}}}^{\gamma\gamma}$  for RP2 and RP4 in this Case also and follows a similar trend in variation with an increase in any of the three CPV phases.

Some particular values corresponding to the benchmark points for the two Cases of this Scenario are given in Tab. 3.

### 4.3 Scenario 3:

Although, as noted earlier, the parameter space corresponding to this Scenario overlaps a little with the Case 2 of Scenario 2, some significant differences are noticeable. Fig. 5a shows a fluctuation in the number of surviving points with varying  $\phi_\lambda$  and  $\phi_\kappa$  which is unlike any of the Cases discussed so far and is unique to this Scenario. The number of good points first rises sharply and then falls

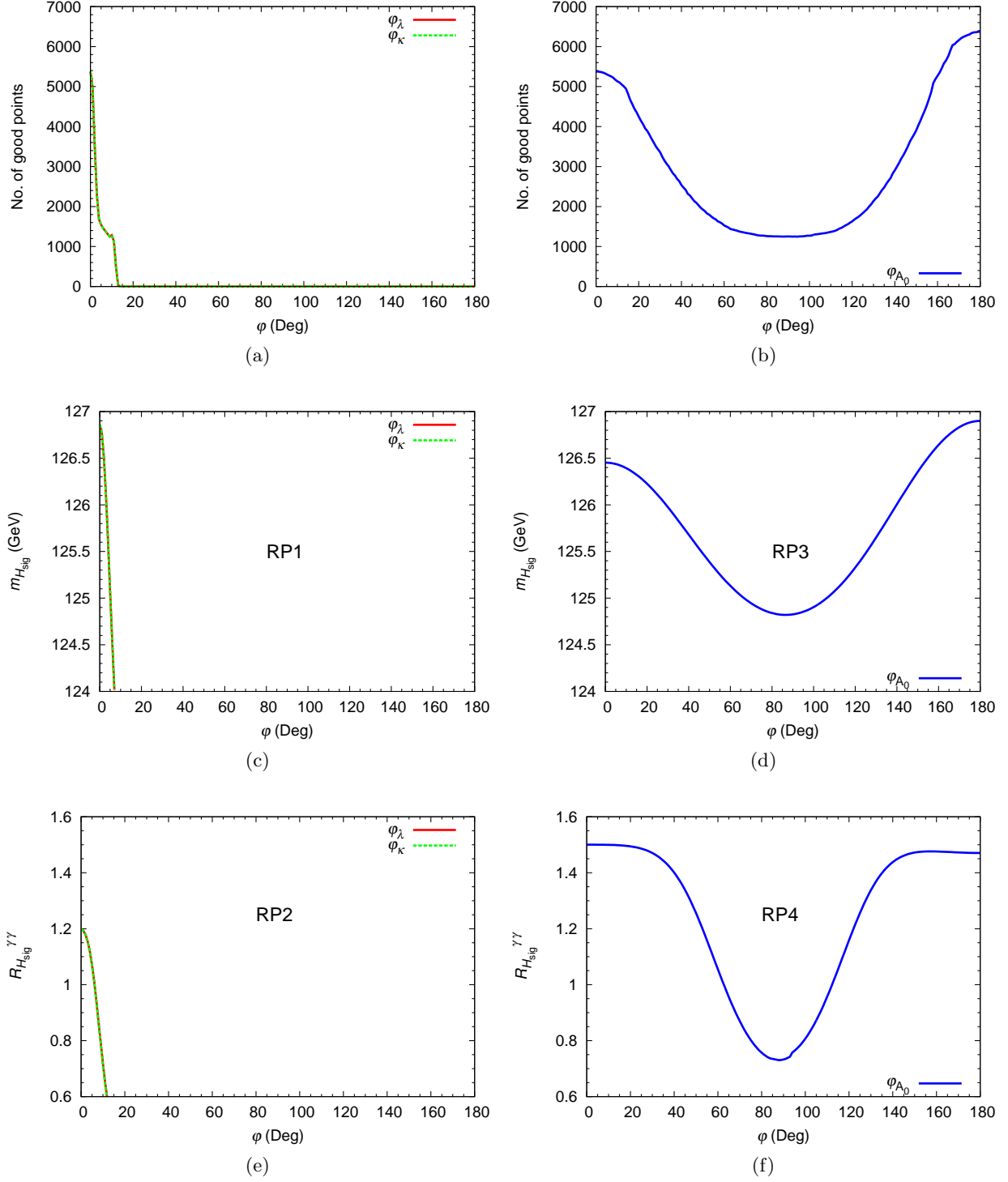


Figure 3: Distributions of good points,  $m_{H_{\text{sig}}}$  and  $R_{H_{\text{sig}}}^{\gamma\gamma}$  for Scenario 2, Case 1.

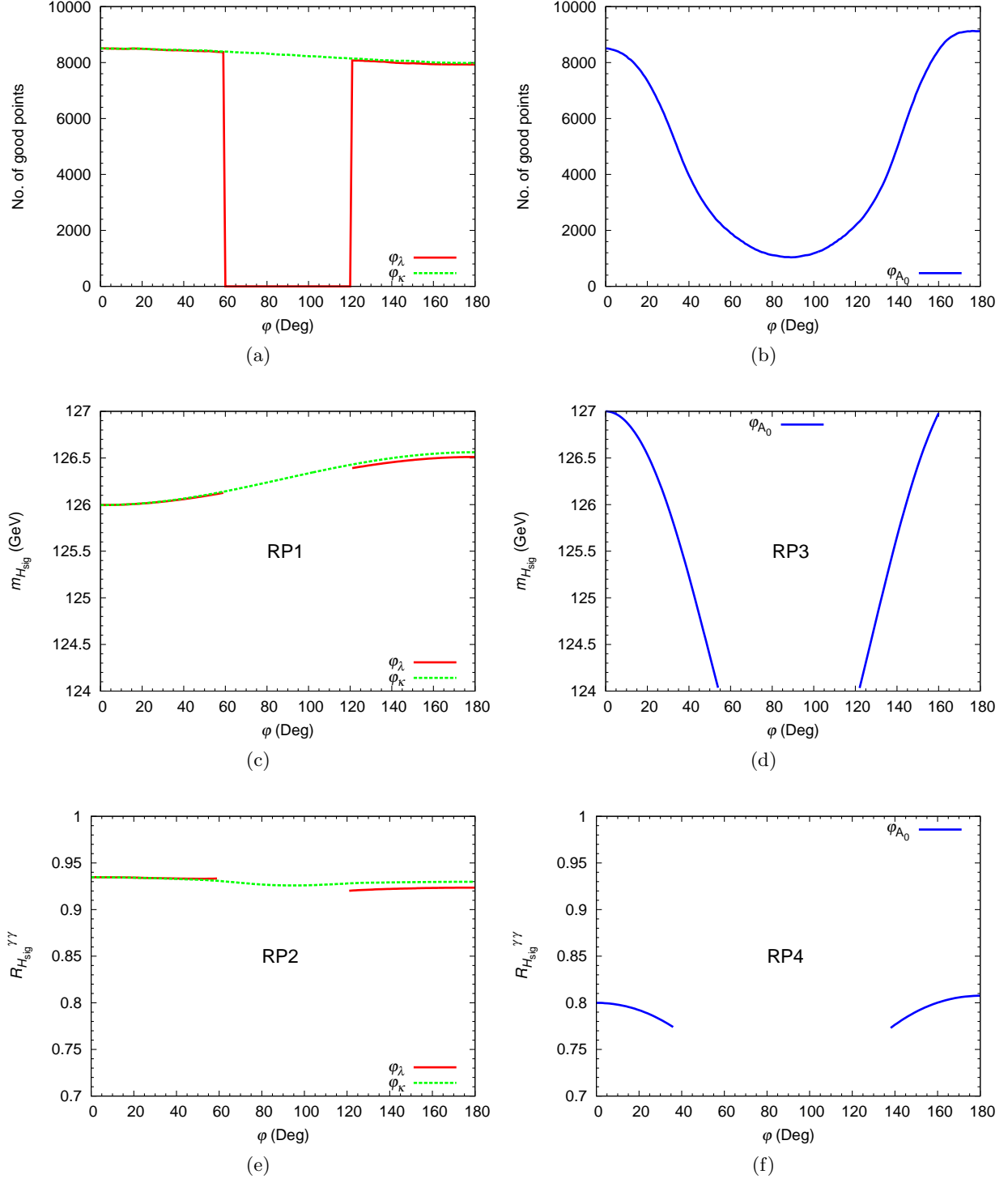


Figure 4: Distributions of good points,  $m_{H_{\text{sig}}}$  and  $R_{H_{\text{sig}}}^{\gamma\gamma}$  for Scenario 2, Case 2.

continuously for  $\phi_\kappa$  between  $\sim 20^\circ$  and  $\sim 80^\circ$ . It then stays almost constant ( $\sim 100$ ) until  $\phi_\kappa \simeq 120^\circ$  and then starts rising sharply again. Note that the number of surviving points never falls to 0 for  $\phi_\kappa$  while it does so for  $\phi_\lambda$  between  $44^\circ$  and  $135^\circ$ , for the same reason as in Case 2 of Scenario 2. Outside this gap the lines corresponding to  $\phi_\lambda$  and  $\phi_\kappa$  overlap each other almost completely. Although the behavior of the number of surviving points in this Scenario is unique, the reason for it is in fact a behavior of both  $m_{H_{\text{sig}}}$  and  $R_{H_{\text{sig}}}^{\gamma\gamma}$  similar, but much more pronounced, to that observed in Case 2 of Scenario 2, as we shall explain below. Fig. 5b shows a trend similar to Scenario 2 for the number of surviving points with increasing  $\phi_{A_0}$ , except that the former dips to 0 for a small intermediate range of the latter. The representative points of this Scenario have the following co-ordinates.

Point	$\lambda$	$\kappa$	$A_\lambda$ (GeV)	$A_\kappa$ (GeV)
RP1	0.195	0.09	1050	-74.5
RP2	0.226	0.06	972	-90.0
RP3	0.226	0.10	950	-81.1
RP4	0.216	0.08	950	-85.6

Fig. 5c for RP1 shows that  $m_{H_{\text{sig}}}$  rises very sharply with increasing  $\phi_\lambda$  and  $\phi_\kappa$  compared to the corresponding point of Case 2, Scenario 2, which is a consequence of comparatively larger absolute values of  $\lambda$  (implying larger singlet-doublet mixing) and  $\kappa$ . In Fig. 5d for RP3 a very typical behavior of  $m_{H_{\text{sig}}}$  is seen with increasing  $\phi_{A_0}$ . Fig. 5e for RP2 shows a behavior of  $R_{H_{\text{sig}}}^{\gamma\gamma}$  much more analogous to that seen for RP2 of Case 1 than of Case 2 of Scenario 2 due, again, to the large absolute value of  $\lambda$  involved. Note, however, the comparatively much smaller value, when CP is conserved, of  $R_{H_{\text{sig}}}^{\gamma\gamma}$ , which further falls sharply with increasing amount of CP-violation. A small value of  $R_{H_{\text{sig}}}^{\gamma\gamma}$  and minimal variation in it with varying  $\phi_{A_0}$  (in its range allowed by the condition on  $m_{H_{\text{sig}}}$ ) is also seen for RP4 in Fig. 5f. Although the maximum values of  $R_{H_{\text{sig}}}^{\gamma\gamma}$  obtainable for this Scenario still agree well with the central value measured at the CMS, the fact that it drops sharply with non-zero CPV phases implies that quite like the other parameters corresponding to this Scenario the CPV phases are also much more fine-tuned than the other two Scenarios.

The very sharp rise in  $m_{H_{\text{sig}}}$  and the steep drop in  $R_{H_{\text{sig}}}^{\gamma\gamma}$  for most of the points are together responsible for the overall behavior of the number of surviving points noticed above. For small values of  $\phi_\lambda/\phi_\kappa$   $m_{H_3}$  rises above the imposed lower limit on  $m_{H_{\text{sig}}}$  for some points which violate this limit in the CPC case. However, while  $m_{H_3}$  increases  $R_{H_{\text{sig}}}^{\gamma\gamma}$  corresponding to these points falls with increasing  $\phi_\lambda/\phi_\kappa$ . Beyond a certain value of  $\phi_\lambda/\phi_\kappa$  not only do the points which previously fell within the limits on  $m_{H_{\text{sig}}}$  and  $R_{H_{\text{sig}}}^{\gamma\gamma}$  start falling out but also the potential new points which now have  $m_{H_{\text{sig}}}$  above the lower limit, have too low a  $R_{H_{\text{sig}}}^{\gamma\gamma}$  to satisfy the limit on it. Hence, the overall number of surviving points starts dropping. After  $\phi_\lambda/\phi_\kappa = 90^\circ$  the behavior of  $m_{H_3}$  is reversed, in analogy with what was observed in Scenario 1 for  $m_{H_1}$ , so that it starts rising slowly again and consequently the number of surviving points starts increasing also.

As with all the other Cases with a  $H_{dR}$ -like  $H_{\text{sig}}$ ,  $R_{H_{\text{sig}}}^{ZZ}$  has similar values as  $R_{H_{\text{sig}}}^{\gamma\gamma}$  when the CPV phases are zero and a similar behavior when these phases are varied. Finally, some details relevant to the four RPs of this Scenario are given in Tab. 3.

## 5 Summary

In summary, we have demonstrated that the CPV NMSSM offers some interesting solutions to the LHC Higgs boson data, which differ substantially from well-known configurations of the CPC



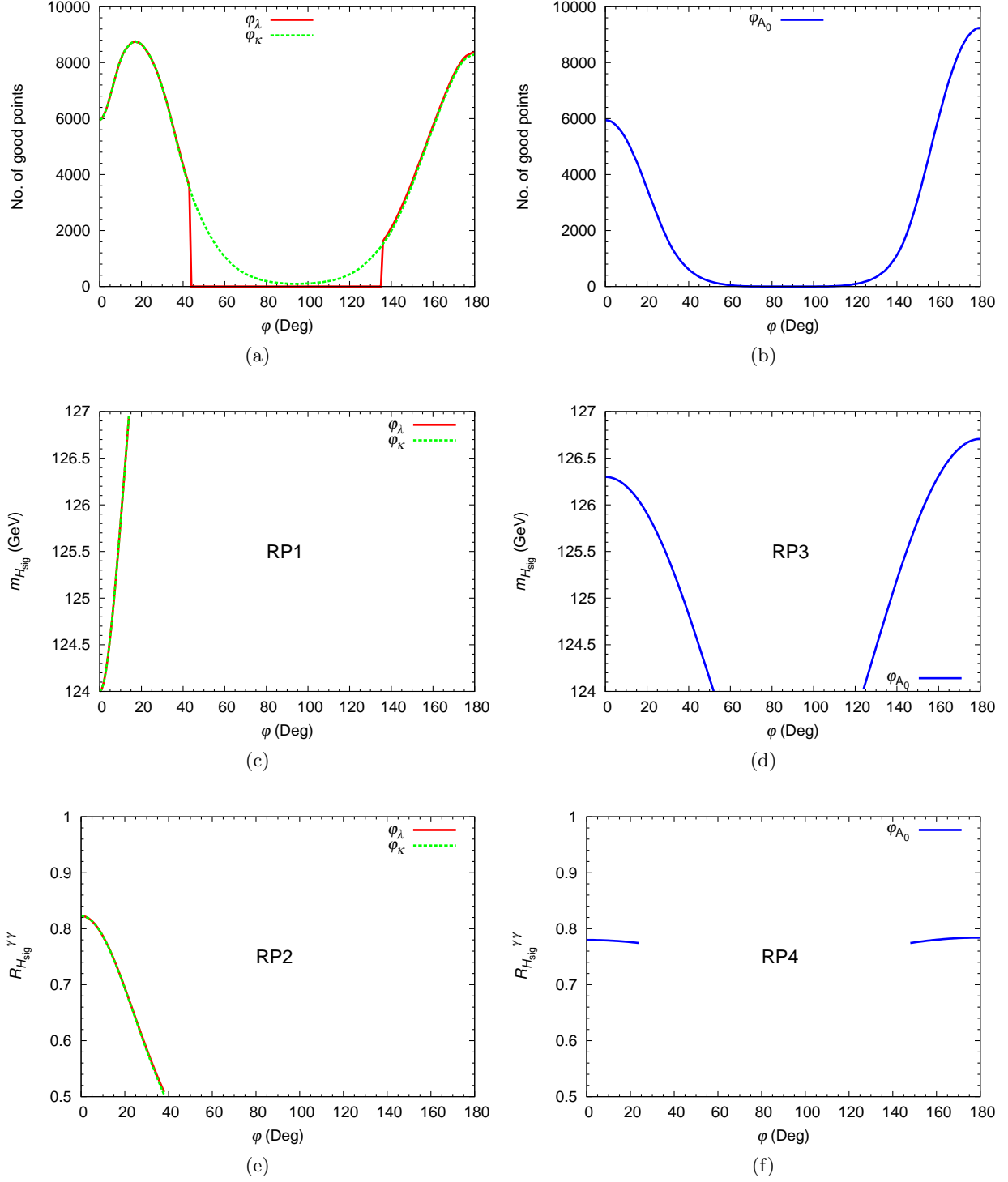


Figure 5: Distributions of good points,  $m_{H_{\text{sig}}}$  and  $R_{H_{\text{sig}}}^{\gamma\gamma}$  for Scenario 3.

Scenario	2, Case 1	2, Case 2	3
Points scanned for each $\phi_\kappa$ or $\phi_\lambda$ or $\phi_{A_0}$	40000		
Points surviving for $\phi_\kappa = \phi_\lambda = \phi_{A_0} = 0$	5377	8506	5944
Min. points surviving, with $\phi_\kappa$	0, 14-180	7979, 180	97, 92-96
Max. points surviving, with $\phi_\kappa$	5377, 0	8506, 0	8763, 17
Min. points surviving, with $\phi_\lambda$	0, 14-180	0, 85-95	0, 44-135
Max. points surviving, with $\phi_\lambda$	5377, 0	8506, 0	8756, 17
$m_{h_{\text{sig}}}$ for RP1 with $\phi_\kappa = \phi_\lambda = 0$	126.8599	125.9949	124.0
$R_{H_{\text{sig}}}^{\gamma\gamma}$ for RP2 with $\phi_\kappa = \phi_\lambda = 0$	1.1976	0.9347	0.8228
Min. $m_{h_{\text{sig}}}$ obtained for RP1, with $\phi_\kappa$	124.0242, 7	125.9949, 0	124.0, 0
Max. $m_{h_{\text{sig}}}$ obtained for RP1, with $\phi_\kappa$	126.8599, 0	126.5612, 180	126.9469, 14
Min. $R_{H_{\text{sig}}}^{\gamma\gamma}$ obtained for RP2, with $\phi_\kappa$	0.5850, 12	0.9259, 91-98	0.5033, 38
Max. $R_{H_{\text{sig}}}^{\gamma\gamma}$ obtained for RP2, with $\phi_\kappa$	1.1976, 0	0.9347, 0	0.8228, 0
Min. $m_{h_{\text{sig}}}$ obtained for RP1, with $\phi_\lambda$	124.0177, 7	125.9949, 0	124.0, 0
Max. $m_{h_{\text{sig}}}$ obtained for RP1, with $\phi_\lambda$	126.8599, 0	126.5107, 180	126.9466, 14
Min. $R_{H_{\text{sig}}}^{\gamma\gamma}$ obtained for RP2, with $\phi_\lambda$	0.5916, 12	0.9202, 121	0.5082, 38
Max. $R_{H_{\text{sig}}}^{\gamma\gamma}$ obtained for RP2, with $\phi_\lambda$	1.1976, 0	0.9347, 0	0.8228, 0
Min. points surviving, with $\phi_{A_0}$	1246, 92	1037, 89	0, 76-100
Max. points surviving, with $\phi_{A_0}$	6372, 180	9120, 180	9241, 180
$m_{h_{\text{sig}}}$ for RP3 with $\phi_{A_0} = 0$	126.9997	126.4522	126.2999
$R_{H_{\text{sig}}}^{\gamma\gamma}$ for RP4 with $\phi_{A_0} = 0$	1.0014	0.7999	0.7799
Min. $m_{h_{\text{sig}}}$ obtained for RP3, with $\phi_{A_0}$	124.0516, 124	124.8208, 87	124.0025, 52
Max. $m_{h_{\text{sig}}}$ obtained for RP3, with $\phi_{A_0}$	127.0, 159	126.8997, 180	126.7063, 180
Min. $R_{H_{\text{sig}}}^{\gamma\gamma}$ obtained for RP4, with $\phi_{A_0}$	0.7304, 88	0.7731, 138	0.7744, 24
Max. $R_{H_{\text{sig}}}^{\gamma\gamma}$ obtained for RP4, with $\phi_{A_0}$	1.5, 0	0.8076, 180	0.7842, 180

Table 3: Scan results for Scenario 2, Cases 1 and 2, and Scenario 3. All angles are in degrees.

NMSSM, thereby augmenting the regions of parameter space which can be scrutinized at the CERN collider. We have concentrated on the case in which only three CPV phases,  $\phi_\kappa$ ,  $\phi_\lambda$  and  $\phi_{A_0}$ , enter the Higgs sector. We have then checked the two-fold impact of these phases, varied separately or simultaneously but always independently from each other, on the mass as well as signal strength of the assumed signal Higgs boson in the  $\gamma\gamma$  decay mode, in different model configurations.

The overall picture that emerges is that any of the three lightest Higgs states of the CPV NMSSM can be the one discovered at the LHC. We have illustrated this by using five benchmark Cases in the parameter space of the model that can easily be adopted for experimental analyses. Our analysis also proves that the possibility of explicitly invoking CPV-phases is not ruled out by the current LHC Higgs boson data in any of our tested plausible NMSSM Scenarios. Finally, a numerical tool for analyzing the Higgs sector of the CPV NMSSM has also been produced and is available upon request. Obvious outlook of this analysis will be to consider the possibility that companion Higgs boson signals to the one extracted at the LHC may emerge in the CPV NMSSM, so as to put the LHC collaborations in the position of confirming or disproving this SUSY hypothesis. An investigation on these lines is now in progress.

## Acknowledgements

S. Moretti is supported in part through the NExT Institute. S. Munir is funded in part by the Wellcome Programme of the Foundation for Polish Science. The work of P. Poulou is partly supported by a SERC, DST (India) project, SR/S2/HEP-41/2009.

## A Mass Matrices

Detailed expressions for the one-loop Higgs boson mass matrices can be found in [28, 29, 30]. Here we only reproduce the tree-level mass matrix to show the dependence on  $\phi_\lambda$  and  $\phi_\kappa$  since the dominant contributions from these phases arise at this level. Note that the tree-level sfermion, neutralino and chargino mass matrices given below are complex by definition. The one-loop effective Higgs potential receives further contributions from  $\phi_\lambda$  and  $\phi_{A_0}$  through the squark and stau sectors and from  $\phi_\lambda$  and  $\phi_\kappa$  through the neutralino and chargino sectors.

- The neutral Higgs boson mass matrix may be written as:

$$\mathcal{M}_H^2 = \begin{pmatrix} \mathcal{M}_S^2 & \mathcal{M}_{SP}^2 \\ (\mathcal{M}_{SP}^2)^T & \mathcal{M}_P^2 \end{pmatrix}. \quad (\text{A.1})$$

Using the minimisation conditions of the Higgs potential, one can define some convenient parameters:

$$\begin{aligned} \mathcal{R} &= |\lambda||\kappa| \cos(\phi'_\lambda - \phi'_\kappa), & \mathcal{I} &= |\lambda||\kappa| \sin(\phi'_\lambda - \phi'_\kappa), \\ R_\lambda &= \frac{|\lambda||A_\lambda|}{\sqrt{2}} \cos(\phi'_\lambda + \phi_{A_\lambda}), & R_\kappa &= \frac{|\kappa||A_\kappa|}{\sqrt{2}} \cos(\phi'_\kappa + \phi_{A_\kappa}), \end{aligned} \quad (\text{A.2})$$

with

$$\phi'_\lambda \equiv \phi_\lambda + \theta + \varphi \quad \text{and} \quad \phi'_\kappa \equiv \phi_\kappa + 3\varphi. \quad (\text{A.3})$$

In terms of these parameters, the entries of the top left  $3 \times 3$  CP-even block in eq. (A.1) are given as

$$\begin{aligned} (\mathcal{M}_S^2)_{11} &= \frac{g_2^2 + g_1^2}{4} v_d^2 + \left( R_\lambda + \frac{1}{2} \mathcal{R} v_S \right) \frac{v_u v_S}{v_d}, \\ (\mathcal{M}_S^2)_{22} &= \frac{g_2^2 + g_1^2}{4} v_u^2 + \left( R_\lambda + \frac{1}{2} \mathcal{R} v_S \right) \frac{v_d v_S}{v_u}, \\ (\mathcal{M}_S^2)_{33} &= R_\lambda \frac{v_d v_u}{v_S} + 2|\kappa|^2 v_S^2 - R_\kappa v_S, \\ (\mathcal{M}_S^2)_{12} &= (\mathcal{M}_S^2)_{21} = \left( -\frac{g_2^2 + g_1^2}{4} + |\lambda|^2 \right) v_d v_u - \left( R_\lambda + \frac{1}{2} \mathcal{R} v_S \right) v_S, \\ (\mathcal{M}_S^2)_{13} &= (\mathcal{M}_S^2)_{31} = -R_\lambda v_u + |\lambda|^2 v_d v_S - \mathcal{R} v_u v_S, \\ (\mathcal{M}_S^2)_{23} &= (\mathcal{M}_S^2)_{32} = -R_\lambda v_d + |\lambda|^2 v_u v_S - \mathcal{R} v_d v_S. \end{aligned} \quad (\text{A.4})$$

where  $g_1$  and  $g_2$  are the  $U(1)_Y$  and  $SU(2)_L$  gauge couplings, respectively, and the bottom right  $2 \times 2$  CP-odd block in reads

$$\mathcal{M}_P^2 = \begin{pmatrix} (R_\lambda + \frac{1}{2} \mathcal{R} v_S) \frac{v^2 v_S}{v_d v_u} & (R_\lambda - \mathcal{R} v_S) v \\ (R_\lambda - \mathcal{R} v_S) v & R_\lambda \frac{v_d v_u}{v_S} + 2 \mathcal{R} v_d v_u - 3 R_\kappa v_S \end{pmatrix}. \quad (\text{A.5})$$

Finally, the entries of the off-diagonal block in eq. (A.1), which responsible for mixing between CP-even and CP-odd states, is given as

$$\mathcal{M}_{SP_\beta}^2 = \begin{pmatrix} 0 & -\frac{3}{2}\mathcal{I}sv_u \\ 0 & -\frac{3}{2}\mathcal{I}sv_d \\ \frac{1}{2}\mathcal{I}sv & -2\mathcal{I}v_uv_d \end{pmatrix}. \quad (\text{A.6})$$

- The chargino mass matrix, in the  $(\widetilde{W}^-, \widetilde{H}^-)$  basis, using the convention  $\widetilde{H}_{L(R)}^- = \widetilde{H}_{d(u)}^-$ , can be written as

$$\mathcal{M}_C = \begin{pmatrix} M_2 & \sqrt{2}m_W \cos \beta \\ \sqrt{2}m_W \sin \beta & \frac{|\lambda|v_S}{\sqrt{2}} e^{i\phi'_\lambda} \end{pmatrix}, \quad (\text{A.7})$$

where  $M_1$  and  $M_2$  are the soft gaugino masses and  $m_W$  is the mass of the  $W$  boson. The above matrix is diagonalized by two different unitary matrices as  $C_R \mathcal{M}_C C_L^\dagger = \text{diag}\{m_{\widetilde{\chi}_1^\pm}, m_{\widetilde{\chi}_2^\pm}\}$ , where  $m_{\widetilde{\chi}_1^\pm} \leq m_{\widetilde{\chi}_2^\pm}$ .

- The neutralino mass matrix, in the  $(\widetilde{B}, \widetilde{W}^0, \widetilde{H}_d^0, \widetilde{H}_u^0, \widetilde{S})$  basis, can be written as

$$\mathcal{M}_N = \begin{pmatrix} M_1 & 0 & -m_Z \cos \beta s_W & m_Z \sin \beta s_W & 0 \\ & M_2 & m_Z \cos \beta c_W & -m_Z \sin \beta c_W & 0 \\ & & 0 & -\frac{|\lambda|v_S}{\sqrt{2}} e^{i\phi'_\lambda} & -\frac{|\lambda|v_S}{\sqrt{2}} e^{i\phi'_\lambda} \\ & & & 0 & -\frac{|\lambda|v \cos \beta}{\sqrt{2}} e^{i\phi'_\lambda} \\ & & & & \sqrt{2}|\kappa|v_S e^{i\phi'_\kappa} \end{pmatrix}. \quad (\text{A.8})$$

with  $m_Z$  being the  $Z$  boson mass,  $s_W = \sin \theta_W$  and  $c_W = \cos \theta_W$ . This matrix is diagonalized as  $N^* \mathcal{M}_N N^\dagger = \text{diag}(m_{\widetilde{\chi}_1^0}, m_{\widetilde{\chi}_2^0}, m_{\widetilde{\chi}_3^0}, m_{\widetilde{\chi}_4^0}, m_{\widetilde{\chi}_5^0})$ , where  $N$  is a unitary matrix and  $m_{\widetilde{\chi}_1^0} \leq m_{\widetilde{\chi}_2^0} \leq m_{\widetilde{\chi}_3^0} \leq m_{\widetilde{\chi}_4^0} \leq m_{\widetilde{\chi}_5^0}$ .

- For the stop, sbottom and stau matrices, in the  $(\widetilde{q}_L, \widetilde{q}_R)$  basis, we have

$$\begin{aligned} \widetilde{\mathcal{M}}_t^2 &= \begin{pmatrix} M_{\widetilde{Q}_3}^2 + m_t^2 + \cos 2\beta m_Z^2 (\frac{1}{2} - \frac{2}{3}s_W^2) & h_t^* v_u (|A_t| e^{-i(\theta+\phi_{A_t})} - \frac{|\lambda|v_S}{\sqrt{2}} e^{i\phi'_\lambda} \cot \beta) / \sqrt{2} \\ h_t v_u (|A_t| e^{i(\theta+\phi_{A_t})} - \frac{|\lambda|v_S}{\sqrt{2}} e^{-i\phi'_\lambda} \cot \beta) / \sqrt{2} & M_{\widetilde{U}_3}^2 + m_t^2 + \cos 2\beta m_Z^2 Q_t s_W^2 \end{pmatrix}, \\ \widetilde{\mathcal{M}}_b^2 &= \begin{pmatrix} M_{\widetilde{Q}_3}^2 + m_b^2 + \cos 2\beta m_Z^2 (-\frac{1}{2} + \frac{1}{3}s_W^2) & h_b^* v_d (|A_b| e^{-i\phi_{A_b}} - \frac{|\lambda|v_S}{\sqrt{2}} e^{i\phi'_\lambda} \tan \beta) / \sqrt{2} \\ h_b v_d (|A_b| e^{i\phi_{A_b}} - \frac{|\lambda|v_S}{\sqrt{2}} e^{-i\phi'_\lambda} \tan \beta) / \sqrt{2} & M_{\widetilde{D}_3}^2 + m_b^2 + \cos 2\beta m_Z^2 Q_b s_W^2 \end{pmatrix}, \\ \widetilde{\mathcal{M}}_\tau^2 &= \begin{pmatrix} M_{\widetilde{L}_3}^2 + m_\tau^2 + \cos 2\beta m_Z^2 (s_W^2 - 1/2) & h_\tau^* v_d (|A_\tau| e^{-i\phi_{A_\tau}} - \frac{|\lambda|v_S}{\sqrt{2}} e^{i\phi'_\lambda} \tan \beta) / \sqrt{2} \\ h_\tau v_d (|A_\tau| e^{i\phi_{A_\tau}} - \frac{|\lambda|v_S}{\sqrt{2}} e^{-i\phi'_\lambda} \tan \beta) / \sqrt{2} & M_{\widetilde{E}_3}^2 + m_\tau^2 - \cos 2\beta m_Z^2 s_W^2 \end{pmatrix}, \end{aligned} \quad (\text{A.9})$$

where  $m_t$ ,  $m_b$  and  $m_\tau$  are the masses of  $t$ ,  $b$  quarks and  $\tau$  lepton, respectively, and  $y_t$ ,  $y_b$  and  $y_\tau$  are the corresponding Yukawa couplings.  $Q_t$  and  $Q_b$  are the respective electric charges of the  $t$  and  $b$  quarks. The mass eigenstates of top and bottom squarks and stau are obtained by diagonalizing the above mass matrices as  $U^{f\dagger} \widetilde{\mathcal{M}}_f^2 U^f = \text{diag}(m_{\widetilde{f}_1}^2, m_{\widetilde{f}_2}^2)$ , such that  $m_{\widetilde{f}_1}^2 \leq m_{\widetilde{f}_2}^2$ , for  $f = t, b, \tau$ .

## References

- [1] ATLAS Collaboration, Phys. Lett. B **716**, 1 (2012).
- [2] CMS Collaboration, Phys. Lett. B **716**, 30 (2012).
- [3] CMS Collaboration, CMS-PAS-HIG-12-045 and CMS-PAS-HIG-12-053.
- [4] ATLAS Collaboration, ATLAS-CONF-2012-162.
- [5] CMS Collaboration, CMS-PAS-HIG-13-001, CMS-PAS-HIG-13-002, CMS-PAS-HIG-13-004 and CMS-PAS-HIG-13-005.
- [6] ATLAS Collaboration, ATLAS-CONF-2013-029 and ATLAS-CONF-2013-030.
- [7] See <http://moriond.in2p3.fr>.
- [8] Z. Kunszt, S. Moretti and W.J. Stirling, Z. Phys. C **74**, 479 (1997).
- [9] CDF and D0 Collaborations, Phys. Rev. Lett. **109**, 071804 (2012)
- [10] E. Accomando *et al.*, arXiv:hep-ph/0608079.
- [11] M. Carena, S. Gori, N. R. Shah and C. E. M. Wagner, JHEP **1203**, 014 (2012); S. Heinemeyer, O. Stal and G. Weiglein, Phys. Lett. B **710**, 201 (2012); A. Arbey *et al.*, Phys. Lett. B **708**, 162 (2012); L. J. Hall, D. Pinner and J. T. Ruderman, JHEP **1204**, 131 (2012); P. Draper *et al.*, Phys. Rev. D **85**, 095007 (2012) G. Guo, B. Ren and X. G. He, arXiv:1112.3188 [hep-ph]; X. G. He, B. Ren and J. Tandean, Phys. Rev. D **85**, 093019 (2012) A. Djouadi, *et al.*, Phys. Lett. B **709**, 65 (2012); B. Batell, S. Gori and L. -T. Wang, JHEP **1206**, 172 (2012) T. Li, J. A. Maxin, D. V. Nanopoulos and J. W. Walker, Phys. Lett. B **710**, 207 (2012); J. -J. Cao, Z. -X. Heng, J. M. Yang, Y. -M. Zhang and J. -Y. Zhu, JHEP **1203**, 086 (2012); M. Carena, I. Low and C. E. M. Wagner, JHEP **1208**, 060 (2012); A. Arbey, M. Battaglia, A. Djouadi and F. Mahmoudi, JHEP **1209**, 107 (2012); K. Schmidt-Hoberg and F. Staub, JHEP **1210**, 195 (2012); Z. Heng, arXiv:1210.3751 [hep-ph]; M. Drees, Phys. Rev. D **86**, 115018 (2012); A. Arbey, M. Battaglia, A. Djouadi and F. Mahmoudi, Phys. Lett. B **720**, 153 (2013) P. Bechtle, S. Heinemeyer, O. Stal, T. Stefaniak, G. Weiglein and L. Zeune, Eur. Phys. J. C **73**, 2354 (2013) K. Schmidt-Hoberg, F. Staub and M. W. Winkler, JHEP **1301**, 124 (2013); M. Carena, S. Gori, I. Low, N. R. Shah and C. E. M. Wagner, JHEP **1302**, 114 (2013); T. Han, Z. Liu and A. Natarajan, arXiv:1303.3040 [hep-ph];
- [12] J. Cao, Z. Heng, D. Li and J. M. Yang, Phys. Lett. B **710**, 665 (2012); H. Baer, V. Barger, A. Mustafayev, Phys. Rev. D **85**, 075010 (2012); L. Aparicio, D. G. Cerdeno and L. E. Ibanez, JHEP **1204**, 126 (2012); J. Ellis and K. A. Olive, Eur. Phys. J. C **72**, 2005 (2012) H. Baer, V. Barger and A. Mustafayev, JHEP **1205**, 091 (2012) N. Desai, B. Mukhopadhyaya and S. Niyogi, arXiv:1202.5190 [hep-ph]; A. Fowlie, M. Kazana, K. Kowalska, S. Munir, L. Roszkowski, E. M. Sessolo, Y.-L. S. Tsai and S. Trojanowski, Phys. Rev. D **86**, 075010 (2012).
- [13] U. Ellwanger, JHEP **1203**, 044 (2012).
- [14] O. Stal and G. Weiglein, JHEP **1201**, 071 (2012) S. F. King, M. Mühlleitner and R. Nevzorov, Nucl. Phys. B **860**, 207 (2012); J. F. Gunion, Y. Jiang and S. Kraml, Phys. Lett. B **710**,

- 454 (2012); U. Ellwanger and C. Hugonie, *Adv. High Energy Phys.* **2012**, 625389 (2012); J. F. Gunion, Y. Jiang and S. Kraml, *Phys. Rev. D* **86**, 071702 (2012); J. F. Gunion, Y. Jiang and S. Kraml, *Phys. Rev. Lett.* **110**, 051801 (2013); G. Belanger, U. Ellwanger, J. F. Gunion, Y. Jiang and S. Kraml, arXiv:1208.4952 [hep-ph]; G. Belanger, U. Ellwanger, J. F. Gunion, Y. Jiang, S. Kraml and J. H. Schwarz, *JHEP* **1301**, 069 (2013); S. F. King, M. Mühlleitner, R. Nevzorov and K. Walz, *Nucl. Phys. B* **870**, 323 (2013); H. K. Dreiner, F. Staub and A. Vicente, *Phys. Rev. D* **87**, 035009 (2013); T. Gherghetta, B. von Harling, A. D. Medina and M. A. Schmidt, *JHEP* **1302**, 032 (2013); D. G. Cerdeno, P. Ghosh and C. B. Park, *JHEP* **1306**, 031 (2013) D. Das, U. Ellwanger and A. M. Teixeira, *JHEP* **1304**, 117 (2013) N. D. Christensen, T. Han, Z. Liu and S. Su, arXiv:1303.2113 [hep-ph]; W. Wang, J. M. Yang and L. L. You, arXiv:1303.6465 [hep-ph]; T. Cheng, J. Li, T. Li and Q. -S. Yan, arXiv:1304.3182 [hep-ph]; R. Barbieri, D. Buttazzo, K. Kannike, F. Sala and A. Tesi, *Phys. Rev. D* **87**, **115018** (2013) M. Badziak, M. Olechowski and S. Pokorski, *JHEP* **1306**, 043 (2013) S. Munir, L. Roszkowski and S. Trojanowski, arXiv:1305.0591 [hep-ph].
- [15] K. Kowalska, S. Munir, L. Roszkowski, E. M. Sessolo, S. Trojanowski and Y. -L. S. Tsai, *Phys. Rev. D* **87**, 115010 (2013)
- [16] P. Athron, S. F. King, D. J. Miller, S. Moretti and R. Nevzorov, *Phys. Rev. D* **86**, 095003 (2012).
- [17] A. Elsayed, S. Khalil and S. Moretti, *Phys. Lett. B* **715**, 208 (2012); L. Basso and F. Staub, *Phys. Rev. D* **87**, 015011 (2013)
- [18] T. Ibrahim and P. Nath, *Rev. Mod. Phys.* **80**, 577 (2008).
- [19] S.-Y. Choi, K. Hagiwara and J.S. Lee, *Phys. Rev. D* **64**, 032004 (2001) and *Phys. Lett. B* **529**, 212 (2002); A.G. Akeroyd and A. Arhrib, *Phys. Rev. D* **64**, 095018 (2001); A. Arhrib, D. K. Ghosh and O.C.W. Kong, *Phys. Lett. B* **537**, 217 (2002); S.Y. Choi, M. Drees, J.S. Lee and J. Song, *Eur. Phys. J. C* **25**, 307 (2002); D. K. Ghosh, R. Godbole, and D. Roy, *Phys. Lett. B* **628**, 131 (2005); D. K. Ghosh, S. Moretti, *Eur. Phys. J. C* **42**, 341 (2005); R.M. Godbole, S. Kraml, S.D. Rindani and R.K. Singh, *Phys. Rev. D* **74**, 095006 (2006); F. Deppisch and O. Kittel, *JHEP* **0909**, 110 (2009) [Erratum-*ibid.* **1003**, 091 (2010)]; K.E. Williams, H. Rzehak and G. Weiglein, *Eur. Phys. J. C* **71**, 1669 (2011); B. Bhattacharjee, A. Chakraborty, D. K. Ghosh and S. Raychaudhuri, *Phys. Rev. D* **86**, 075012 (2012).
- [20] M. S. Carena, J. R. Ellis, A. Pilaftsis and C. E. M. Wagner, *Phys. Lett. B* **495**, 155 (2000). J. R. Ellis, J. S. Lee and A. Pilaftsis, *Phys. Rev. D* **72**, 095006 (2005);
- [21] For a review of MSSM Higgs phenomenology see: S. Y. Choi, J. Kalinowski, Y. Liao and P. M. Zerwas, *Eur. Phys. J. C* **40**, 555 (2005); J. R. Ellis, J. S. Lee and A. Pilaftsis, *Phys. Rev. D* **70**, 075010 (2004); M. S. Carena, J. R. Ellis, A. Pilaftsis and C. E. M. Wagner, *Nucl. Phys. B* **625**, 345 (2002); M. Carena *et al.*, arXiv:hep-ph/0010338; S.Y. Choi, M. Drees and J.S. Lee, *Phys. Lett. B* **481**, 57 (2000); G.L. Kane and L.-T. Wang, *Phys. Lett. B* **488**, 383 (2000); A. Pilaftsis and C.E.M. Wagner, *Nucl. Phys. B* **553**, 3 (1999); D.A. Demir, *Phys. Rev. D* **60**, 055006 (1999); A. Pilaftsis, *Phys. Rev. D* **58**, 096010 (1998) and *Phys. Lett. B* **435**, 88 (1998); M. S. Carena, M. Quiros and C. E. M. Wagner, *Nucl. Phys. B* **461**, 407 (1996); M. S. Carena, J. R. Espinosa, M. Quiros and C. E. M. Wagner, *Phys. Lett. B* **355**, 209 (1995).

- [22] A. Pilaftsis and C. E. M. Wagner, Nucl. Phys. B **553**, 3 (1999); M. Carena, J.R. Ellis, A. Pilaftsis and C.E.M. Wagner, Phys. Lett. B **495**, 155, (2000) and Nucl. Phys. B **586**, 92 (2000).
- [23] V. Cirigliano, Y. Li, S. Profumo and M. J. Ramsey-Musolf, JHEP **1001**, 002 (2010).
- [24] Phys. Rev. Lett. **84**, 22 (2000) and A. Dedes and S. Moretti, Nucl. Phys. B **576**, 29 (2000) .
- [25] S. Hesselbach, S. Moretti, S. Munir and P. Poulose, J. Phys. Conf. Ser. **335**, 012020 (2011); AIP Conf. Proc. **1200**, 498 (2010); Phys. Rev. D **82**, 074004 (2010); arXiv:0710.4923 [hep-ph]; J. Phys. Conf. Ser. **110**, 072017 (2008) and Eur. Phys. J. C **54**, 129 (2008); S. Moretti, S. Munir and P. Poulose, Phys. Lett. B **649**, 206 (2007).
- [26] A. Chakraborty, B. Das, J. L. Diaz-Cruz, D. K. Ghosh, S. Moretti and P. Poulose, arXiv:1301.2745 [hep-ph].
- [27] M. Maniatis, Int. J. Mod. Phys. A **25**, 3505 (2010).
- [28] K. Cheung, T. -J. Hou, J. S. Lee and E. Senaha, Phys. Rev. D **82**, 075007 (2010).
- [29] T. Graf, R. Grober, M. Mühlleitner, H. Rzehak and K. Walz, JHEP **1210**, 122 (2012).
- [30] K. Funakubo and S. Tao, Prog. Theor. Phys. **113**, 821 (2005).
- [31] J. S. Lee, M. Carena, J. Ellis, A. Pilaftsis and C. E. M. Wagner, Comput. Phys. Commun. **184**, 1220 (2013) Comput. Phys. Commun. **180**, 312 (2009); J. S. Lee, A. Pilaftsis, M. S. Carena, S. Y. Choi, M. Drees, J. R. Ellis and C. E. M. Wagner, Comput. Phys. Commun. **156**, 283 (2004).
- [32] K. Cheung, T. -J. Hou, J. S. Lee and E. Senaha, Phys. Rev. D **84**, 015002 (2011).
- [33] S. Munir, in preparation.
- [34] U. Ellwanger, C. Hugonie and A. M. Teixeira, Phys. Rep. **496**, 1 (2010).
- [35] <http://www.th.u-psud.fr/NMHDECAY/nmssmtools.html>; U. Ellwanger, J. F. Gunion and C. Hugonie, JHEP **0502**, 066 (2005); U. Ellwanger and C. Hugonie, Comput. Phys. Commun. **175**, 290 (2006).
- [36] S. Chatrchyan *et al.* [CMS Collaboration], Phys. Rev. Lett. **110**, 081803 (2013).
- [37] A. Djouadi and G. Moreau, arXiv:1303.6591 [hep-ph].
- [38] C. A. Baker, D. D. Doyle, P. Geltenbort, K. Green, M. G. D. van der Grinten, P. G. Harris, P. Iaydjiev and S. N. Ivanov *et al.*, Phys. Rev. Lett. **97**, 131801 (2006).
- [39] E. D. Commins, J. Phys. Soc. Jap. **76**, 111010 (2007).
- [40] W. C. Griffith, M. D. Swallows, T. H. Loftus, M. V. Romalis, B. R. Heckel and E. N. Fortson, Phys. Rev. Lett. **102**, 101601 (2009).
- [41] A. Pilaftsis and C. E. M. Wagner, Nucl. Phys. B **553**, 3 (1999); M. S. Carena, J. R. Ellis, A. Pilaftsis and C. E. M. Wagner, Nucl. Phys. B **586**, 92 (2000); S. Abel, S. Khalil and O. Lebedev, Nucl. Phys. B **606**, 151 (2001).

- [42] N. Haba, Prog. Theor. Phys. **97**, 301 (1997); T. Ibrahim and P. Nath, Phys. Rev. D **58**, 111301 (1998) [Erratum-ibid. D **60**, 099902 (1999)]; M. Boz, Mod. Phys. Lett. A **21**, 243 (2006); . R. Ellis, J. S. Lee and A. Pilaftsis, JHEP **0810**, 049 (2008); Y. Li, S. Profumo and M. Ramsey-Musolf, JHEP **1008**, 062 (2010).
- [43] J. Beringer *et al.* [Particle Data Group Collaboration], Phys. Rev. D **86**, 010001 (2012).